EurJIC
European Journal of Inorganic Chemistry

Research Article
doi.org/10.1002/ejic.202200478

Chemistry Europe
European Chemical Societies Publishing

www.eurjic.org

Experimental and Theoretical Evaluation of Four NLO-Active Divalent Transition-Metal Complexes Supported by an Enantiomerically Pure Tetradentate Schiff Base Ligand

Salvador Celedón,*[a, e] Paul Hamon,[b] Vania Artigas,[c] Mauricio Fuentealba,[c] Samia Kahlal,[b] Isabelle Ledoux-Rak,[d] David Carrillo,[a] Jean-Yves Saillard,[b] Carolina Manzur,*[a] and Jean-René Hamon*[b]

This paper reports on a series of five chiral Schiff base push-pull compounds derived from enantiomerically pure (1*R*,2*R*)-(−)-1,2-diaminocyclohexane. The Ni^{II}, Cu^{II}, Zn^{II} and Pd^{II} complexes supported by a ferrocene-containing unsymmetrically-substituted N_2O_2 quadridentate Schiff base ligand were prepared via template reactions and isolated in 74–87% yields. A combination of EA, IR, UV/vis and $^{1}H/^{13}C\{^{1}H\}$ NMR spectroscopy, HRMS spectrometry, cyclic voltammetry and single-crystal X-ray analysis (for the proligand **2** and its Ni^{II} derivative **3**), together with computational methods (DFT and TD-DFT) was used to fully characterize and study the properties of all products. Both **2** and **3** crystallize in the orthorhombic non-centrosymmetric space group $P2_12_12_1$, with two (*R*,*R*)-(−)-chiral carbon atoms in their structure. Second-order nonlinear polarizabilities β have been measured by using Harmonic Light Scattering at 1.91 μm, with the Pd(II) species showing the higher NLO response of 460×10^{-30} esu.

Introduction

Non-centrosymmetric compounds are of great interest because of their potential applications in many areas such as piezoelectricity, ferroelectricity, pyroelectricity and, especially, second-order nonlinear optical (NLO) materials.[1,2] In the latter case, besides being ordered in a non-centrosymmetric packing, the chromophores must exhibit a molecular hyperpolarizability (β) as large as possible to generate quadratic NLO activity.[3,4] This property exhibited by condensed matter, which has been approached mainly by the incorporation and non-centrosymmetric arrangement of NLO-phores into a macroscopic environment, constitutes a key step toward the engineering of nonlinear materials and devices.[2,4–7] In this regard, several strategies using dipolar chromophores have been intensively investigated, such as statistical orientation by electrical poling of NLO-polymers, stepwise construction of multilayers, supramolecular solid-state assemblies, or preorganization of NLO active species within multichromophoric systems.[5,8–11] On the other hand, coordination complexes featuring a dipolar push-pull structure represent a fascinating and growing class of NLO chromophores due to the presence of low-energy and intense metal-to-ligand or ligand-to-metal charge-transfer transitions which are tunable by virtue of the nature, oxidation states, and coordination sphere of the metal centers.[12–15] Among those inorganic chromophores, transition-metal complexes of Schiff base ligands form a promising and efficient class of NLO molecular materials.[16–21] Complexes based on unsymmetrically-substituted tetradentate N_2O_2 donor Schiff base ligands,[22,23] showing high second-order NLO responses are made of electron-donor group (D) and electron-acceptor group (A) linked through a π-conjugated system to form a D-π-A dipolar push-pull structure in which the metal ion is a constituent of the polarizable bridge.[20,21,24,25] The NLO responses of such molecular species have been measured principally in solution using Electric-Field-Induced Second Harmonic (EFISH)[26] or harmonic light scattering (HLS) techniques,[27] because the large dipole moments typically associated with D-π-A systems, tend to favor the anti-parallel alignment of neighboring molecules in the crystal packing, thus canceling out their second-order NLO responses in the solid state.[5,28,29] To overcome this problem, some chemical tools such as the formation of weak bonds, steric factors, molecular

[a] Dr. S. Celedón, Prof. Dr. D. Carrillo, Prof. Dr. C. Manzur
Laboratorio de Química Inorgánica, Instituto de Química,
Facultad de Ciencias, Pontificia Universidad Católica de Valparaíso,
Campus Curauma, Avenida Universidad 330, Valparaíso, Chile
E-mail: sceledn p@edu.udla.cl
cecilia.manzur@pucv.cl
http://www.institutodequimica.ucv.cl/es/
[b] P. Hamon, Dr. S. Kahlal, Prof. Dr. J.-Y. Saillard, Dr. J.-R. Hamon
Univ Rennes, CNRS, ISCR (Institut des Sciences Chimiques de Rennes) – UMR 6226, 35000 Rennes, France
E-mail: jean-rene.hamon@univ-rennes1.fr
http://iscr.univ-rennes1.fr/omc/
[c] Dr. V. Artigas, Prof. Dr. M. Fuentealba
Laboratorio de Cristalografía, Instituto de Química,
Facultad de Ciencias, Pontificia Universidad Católica de Valparaíso,
Campus Curauma, Avenida Universidad 330, Valparaíso, Chile
[d] Prof. Dr. I. Ledoux-Rak
Laboratoire Lumière, Matière et Interfaces,
ENS Paris Saclay, UMR CNRS 9024, Institut d'Alembert, Centrale Supelec,
4 Avenue des Sciences, 91190 Gif-sur-Yvette, France
[e] Dr. S. Celedón
Instituto de Ciencias Naturales, Universidad de las Américas,
Manuel Montt 948, Santiago, Chile
https://cienciasnaturales.udla.cl/

Supporting information for this article is available on the WWW under https://doi.org/10.1002/ejic.202200478

Part of the "Coordination Chemistry Division of the French Chemical Society Prize Winners" Special Collection.

Research Article
doi.org/10.1002/ejic.202200478

chirality, use of ionic species, etc., have been applied.[30] Chirality of salen-type ligand has, indeed, proven to be a useful strategy for engineering the chromophores into acentric crystal structures. This approach is based on the introduction of two asymmetric carbon atoms of a chiral diamine, such as D-(+)- and D,L-camphoric diamine,[31] 1,2-diphenylethylenediamine or 1,2-diaminocyclohexane, to force the crystallization into a noncentrosymmetric space group. This work was pioneered by Lacroix and co-workers with nickel(II) and manganese(III) chiral inorganic chromophores,[32] and extended very recently by Rigamonti *et al.* to copper(II) complexes of chiral push-pull tetradentate Schiff base ligands,[33] providing sizeable solid-state NLO efficiencies, measured by the Kurtz-Perry method,[34] with respect to standard urea. Herein, we aim at exploring the NLO properties of a new family of four divalent transition-metal complexes featuring a chiral unsymmetrically substituted N_2O_2 tetradentate Schiff base ligand, made of a donor ferrocenyl-functionalized redox-active β-keto-enamine[35] linked to an electron withdrawing 5-nitrosalicylaldimine through the enantiomerically pure (1*R*,2*R*)-(−)-1,2-cyclohexane-diyl (abbreviated as *c*-C_6H_{10}). In this sense, we wish to report the synthesis of the diprotic Schiff-base proligand **2** resulting from condensation of the known tridentate N_2O metalloligand precursor (1*R*,2*R*)-[Fc–C(=O)CH=C(CH_3)NH-*c*-C_6H_{10}–NH_2] (**1**, Fc = ferrocenyl=Fe(η^5-C_5H_5) (η^5-C_5H_4))[36] with 5-nitrosalicylaldehyde, and the derived neutral heterobimetallic Schiff base complexes [M{(1*R*,2*R*)-Fc–C(=O)CH=C(CH_3)N-*c*-C_6H_{10}–N=CH–(2-O,5–NO_2–C_6H_3)}] were M=Ni, Cu, Zn and Pd (**3**, **4**, **5** and **6**, respectively, see formulas in Scheme 1 and Scheme 2). The analytical and spectral characterization, and electrochemical properties are reported. Additionally, the crystal and molecular structures of the chiral compounds **2** and **3** were determined by single crystal X-ray diffraction analysis and the electronic structure and optical properties were investigated through DFT and TD-DFT calculations. Finally, second-order nonlinear polarizabilities β of compounds **1–6** have been measured in dichloromethane using the Harmonic Light Scattering (HLS) technique at 1.9 μm.

Results and discussion

Synthesis and characterization

Schiff condensation reaction[37] between the tridentate Schiff-base proligand (1*R*,2*R*)-Fc–C(=O)CH=C(CH_3)NH-*c*-C_6H_{10}–NH_2 (**1**) and an equimolar amount of 2-hydroxy-5-nitrobenzaldehyde afforded the expected diprotic unsymmetrically-substituted tetradentate Schiff base ligand precursor **2**, isolated as a red crystalline product in 87% yield (Scheme 1). Compound **2** exhibits a good solubility in MeOH, EtOH, CH_2Cl_2, $CHCl_3$ and Me_2CO, but is insoluble in non-polar solvents.

The chiral bimetallic Schiff-base complexes **3–6** were prepared via a one-pot template procedure starting from the tridentate proligand **1**, 2-hydroxy-5-nitrobenzaldehyde and hydrated nickel(II), copper(II), zinc(II) and palladium(II) acetates, respectively, under mild conditions, as outlined in Scheme 2. It must be noted that they are also accessible, although in much lower yields, using the stepwise procedure involving the reaction of the Schiff base proligand **2** with the appropriate metal(II) acetate salt $M(OAc)_2{\cdot}xH_2O$. Complexes **3–6** precipitated directly from the reaction mixture and were collected by filtration as microcrystalline solids isolated in 74–86% yields (see Exp. Sect.). Complexes **3–6** are insoluble in diethyl ether

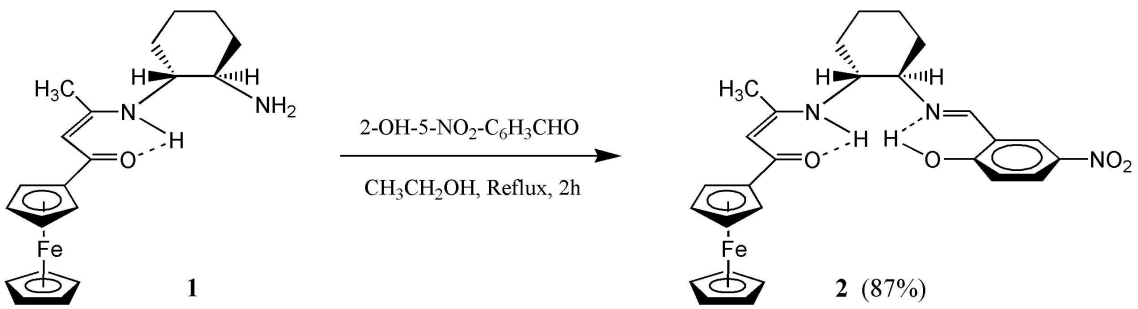

Scheme 1. Synthesis of chiral Schiff base proligand **2**.

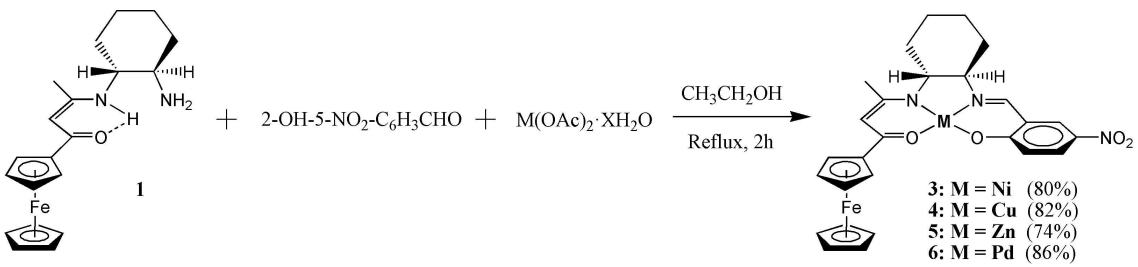

Scheme 2. Synthesis of the chiral heterobimetallic Schiff base complexes **3–6**.

Research Article
doi.org/10.1002/ejic.202200478

and hydrocarbons, poorly soluble in alcohols but soluble in CH_2Cl_2, $CHCl_3$, DMF and DMSO.

The newly prepared compounds **2**–**6** are stable towards air, light and moisture both in solution and in the solid state. Their bulk purity was determined through elemental analysis, and their composition and formulation were established from FT-IR, ultraviolet-visible (UV-Vis) and multinuclear NMR spectroscopy. Molecular structures of compounds **2** and **3** were further confirmed by single crystal X-ray crystallography (see below). Additionally, HRMS positive ESI spectra showed the expected isotopic distribution for the molecular ion peaks $[M]^+$ for all the compounds, along with the sodium aggregate $[M+Na]^+$ for **2**, **3**, **5** and **6** (see the Exp. Sect. and Figures S1–S5 in Supporting Information).

The solid-state FT-IR spectra of the five compounds **2**–**6** are presented in Figures S6–S10 (Supporting Information). The spectrum of the proligand **2** exhibits both the ν(O–H) and ν(N–H) stretching vibrations due to the phenol and enamine functionalities at 3432 and 3260 cm^{-1}, respectively (Figure S6). The disappearance of the N–H vibration in the spectra of complexes **3**–**6** (Figures S7–S10) indicates that the macroacyclic N_2O_2 ligand is bonded to the nickel(II), copper(II), zinc(II) and palladium(II) ions through the amino nitrogen atom. The involvement of the phenoxo oxygen atom in coordination is established by ^{1}H NMR spectroscopy and X-ray crystallography (see below), thus achieving a dianionic N_2O_2 complexation type of the tetradentate Schiff base ligand. The persistence of a broad band about 3400 cm^{-1} in the spectra of complexes **3**–**6** is presumably due to some moisture. The $[M(N_2O_2)]$ complexation mode in **3**–**6** species is further confirmed by the vibrational absorption frequencies observed in the range 577–540 cm^{-1} that are associated with the ν(M–O) vibration and those seen in the range 494–423 cm^{-1} that can be assigned to ν(M–N) stretching mode.[38] On the other hand, the spectra of **2**–**6** show the presence of a set of medium to strong intensity bands in the 1639–1550 cm^{-1} region, assigned to the ν(C=O), ν(C=N) and ν(C=C) stretching vibrations of the organic Schiff base skeleton.[39] Moreover, for each compound the nitro substituent group gives rise to well-defined very intense bands in the 1496–1521 and 1302–1321 cm^{-1} ranges, assigned to the asymmetric and symmetric ν(N=O) stretching modes, respectively.[40] For all the compounds, the strong deformation modes of the C–H bonds showed up about 720 cm^{-1}.[38,39]

The ^{1}H and ^{13}C{^{1}H} NMR spectra of the four diamagnetic compounds **2**, **3**, **5** and **6**, recorded in [d_6]-DMSO at 298 K (Figure 1 and Figures S11–S16, Supporting Information), displayed the expected resonance patterns consistent with the proposed structures (see Exp. Sect. for complete assignments). For the four compounds, the assembling of the N_2O_2 macroacyclic Schiff base framework is confirmed by the resonances of the azomethine N=CH protons observed at $\delta = 8.73$ (s), 8.49 (d), 8.74 (s) and 8.67 (d) ppm, respectively; singlet or doublet depends on the resolution of the spectrum, the doublet being due to a $^4J_{H,H}$ with the H-7 proton (see Exp. Sect., Figure 7 for atom labelling). Moreover, in the high field region of the ^{1}H NMR spectra, the aliphatic proton signals corresponding to the chiral (1*R*,2*R*)-cyclohexane-diyl unit are well-resolved and have all been assigned (see Exp. Sect. for details). In addition, the singlets observed in the $\delta = 2.03$–2.32, 4.03–4.23 and 5.24–5.47 ppm ranges with integral ratio 3:5:1 are due to the methyl, unsubstituted cyclopentadienyl ligand and methine protons of the ferrocenyl enamidoketone fragment, respectively.

The protonated Schiff base proligand **2** exists as its enaminone tautomeric form in solution (Figure 1). The ^{1}H NMR spectrum displays a deshielded amino proton doublet at $\delta =$ 10.86 ppm, this deshielding is due to intramolecular hydrogen bonding between the N–H group and the carbonyl oxygen atom.[25a,35a,41] Note also that the most downfield shifted broad singlet appearing at $\delta = 14.40$ ppm is due to the hydroxyl proton engaged in a second intramolecular hydrogen bond with the imine nitrogen atom (Scheme 1).[25a,41,42] As expected, those two signals disappeared upon complexation (Figure 1, Figures S11 and S12), thus confirming coordination of the dianionic tetradentate Schiff base ligand through amino nitrogen and phenolato oxygen atoms.

In the ^{1}H NMR spectra of **2**, **3**, **5** and **6**, resonances of the diastereotopic protons of the substituted cyclopentadienyl ring are observed in the $\delta = 4.36$–4.42 and 4.60–4.76 ppm ranges for H_β and H_α protons, respectively (Figure 1, Figures S11 and S12). Interestingly, for **2** they give rise to two signals integrating each for 2 H, while for the complexed and more rigid species **3**, **5** and **6** they appear as three signals, a broad one for the two H_β protons and two singlets for H_α and $H_{\alpha'}$ (see Exp. Sect. for details). Although the magnetic non-equivalency is only observed for the H_α protons, ther is no doubt that the broad signals contain the two close and overlapping resonances due to H_α and $H_\alpha{}'$ protons.

The ^{13}C{^{1}H} NMR spectra of compounds **2**, **3**, **5** and **6** (Figures S13–S16, Supporting Information) fully reproduce the features observed in ^{1}H NMR and support the interpretation outlined above, clearly demonstrating the asymmetric nature of the four Schiff base derivatives. Interestingly, the two resonances at $\delta = 67.9$ (C_α) and 70.2 (C_β) ppm of the substituted cyclopentadienyl ring carbons observed in the spectrum of proligand **2**, are split into four signals at $\delta = 67.7$ (C_α), 68.0 ($C_{\alpha'}$), 70.1 (C_β) and 70.2 ($C_{\beta'}$) ppm, in the ^{13}C{^{1}H} NMR spectrum of the zinc derivative **5** (Figure S15), thus confirming the magnetic non-equivalency of the cyclopentadienyl carbon nuclei. One can also note that upon complexation, the chemical shift of the carbonyl carbon ($\delta = 190.4$ ppm) in **2** is upfield shifted by about 16 ppm in **3** and **6** while it remains unchanged in the Zn(II) complex **5** (Figures S13–S16). Such upfield shift, although smaller (4–6 ppm) is also noted for the –CH=*C*–N enamido carbon whereas a downfield shift (8–10 ppm) is observed for the N=CH methine carbon (see Exp. Sect. for details). Similar behaviors have previously been observed for Ni(II)/Pd(II) and Zn(II) complexes of N_2O_2 tetradentate Schiff base ligands.[25,36]

Crystal structural studies of Schiff base derivatives 2 and 3

Diffraction-quality single crystals for X-ray structure investigation were simply obtained by cooling to −15 °C the reaction

Research Article
doi.org/10.1002/ejic.202200478

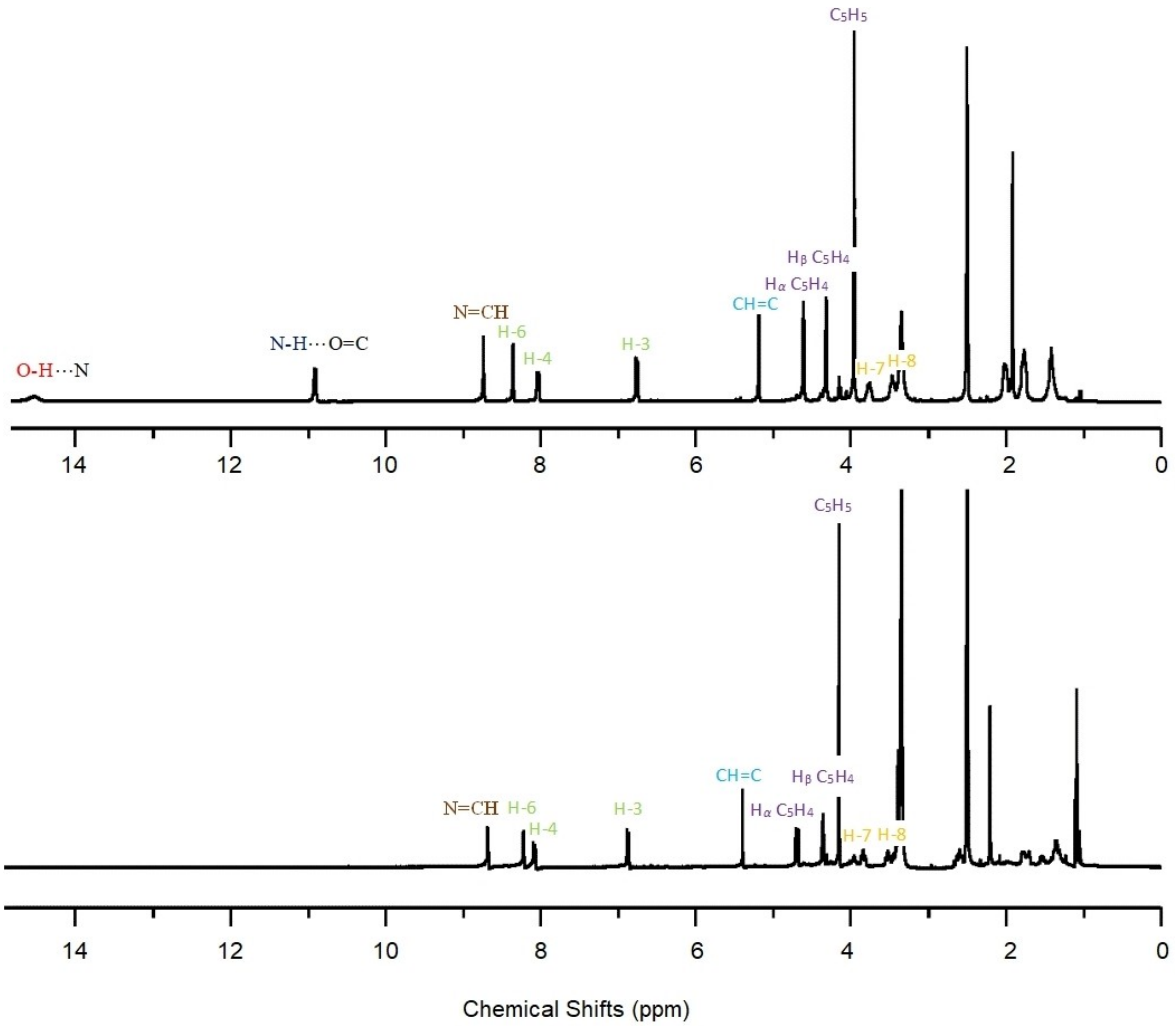

Figure 1. ^{1}H NMR spectra (400 MHz) of metalloligand **2** (top) and of its related Pd(II) complex **6** (bottom), recorded in [d_6]DMSO at 298 K.

mixture for **2**, and by using the slow diffusion crystallization method for **3** (see Exp. Sect.). The molecular structure of the two compounds **2** and **3** are displayed in Figure 2. Bond distances and angles of the first Ni(II) coordination sphere of **3** are given in Table 1, while selected ones of the Schiff base proligand **2** along with those of the Schiff base ligand of **3** are provided in Table S1 (Supporting Information). The two compounds crystallize in the same orthorhombic non-centrosymmetric space group $P2_12_12_1$, with a single molecule in the asymmetric unit in the case of **2**, and two crystallographically nonequivalent molecules (**3 A**, **3B**) in the case of the heterobimetallic species. In the two complexes, the cyclohexane-diyl ring adopts a chair conformation and the ferrocenyl unit features a typical linear η^5-Fe-η^5 sandwich structure, with metrical parameters in agreement with a Fe(II) oxidation state.[43] The cyclopentadienyl rings are parallel, eclipsed (2.4(4)°) in **2** and quasi-eclipsed (10.3(9)° and 9.3(9)°) in **3 A** and **3B**, respectively (Table S2, Supporting Information). In both crystal packing of **2** and **3**, the molecules are loosely connected to one another through weak intermolecular hydrogen bonds (Figures S17 and S18, Tables S3 and S4). The other aspects of the structures are discussed below in two sections for the sake of simplicity.

Table 1. Selected bond distances (Å) and angles (°) for the first Ni(II) coordination sphere of compound **3**.

	3 A	3B
Bond distances		
Ni(1)–O(1)	1.825(4)	1.826(4)
Ni(1)–O(2)	1.849(4)	1.854(4)
Ni(1)–N(1)	1.873(4)	1.870(4)
Ni(1)–N(2)	1.837(4)	1.862(4)
Bond angles		
O(1)–Ni(1)–N(2)	173.8(2)	174.97(18)
O(2)–Ni(1)–N(1)	171.73(19)	173.86(19)
O(1)–Ni(1)–O(2)	81.99(16)	82.84(15)
O(1)–Ni(1)–N(1)	96.68(17)	95.54(17)
O(2)–Ni(1)–N(2)	94.31(18)	94.27(17)
N(1)–Ni(1)–N(2)	87.69(18)	87.76(19)

Proligand 2: The molecular structure of **2** (Figure 2 top) show that it adopts the *Z-s-Z* conformation,[44] consistent with a

Research Article
doi.org/10.1002/ejic.202200478

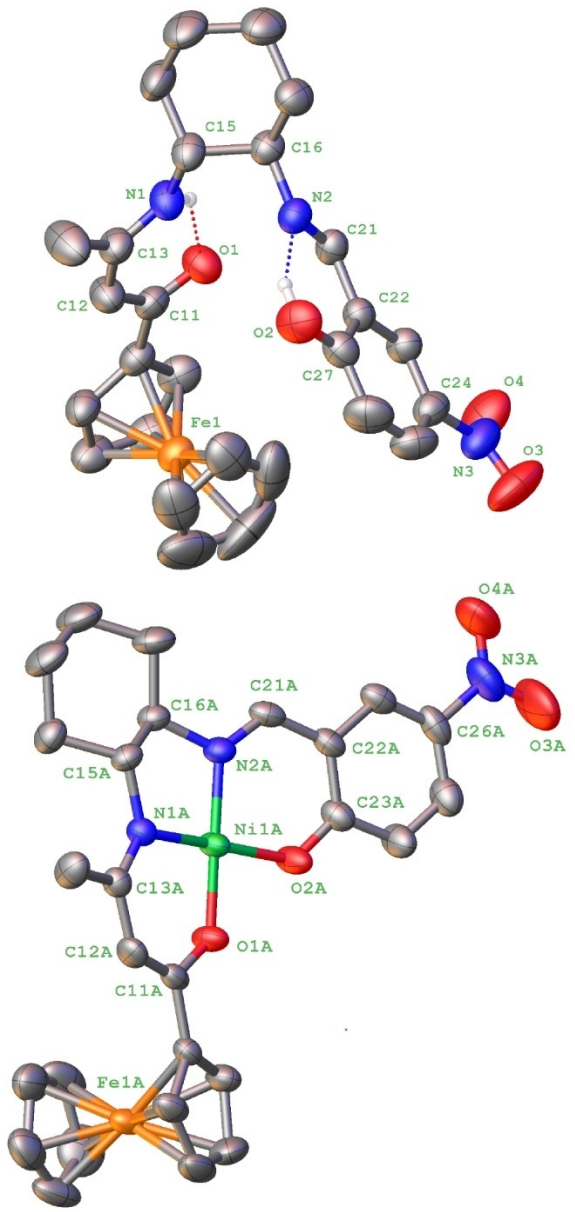

Figure 2. Molecular structures of the chiral Schiff base proligand **2** (top), and of the bimetallic complex **3 A** (bottom) with partial atom numbering schemes. Hydrogen atoms, except those involved in hydrogen bonding interactions in **2**, have been omitted for clarity. Thermal ellipsoids are drawn at 50 % probability.

keto-enamine tautomeric isomer. An intramolecular N(1)–H···O-(1) hydrogen bond with $d_{N\cdots O} = 2.648(3)$ Å (Table S3, Supporting Information), closes the planar pseudo six-membered ring through a resonant ···O(1)=C(11)–C(12)=C(13)–N(1)–H··· fragment,[45] with alternating double-, single-, double- and single-bonds[46] between the vicinal sp^2-hybridized atoms (Table S1, Supporting Information). On the other hand, the potentially tetradentate acyclic metalloligand **2** exhibits a second intramolecular hydrogen bond located between the hydroxo substituent of the salicylidene ring and the imine nitrogen atom with a N(2)···O(2) separation of 2.540(4) Å (Table S3, Supporting Information). The plane of the enaminone core is coplanar with that of the substituted cyclopentadienyl ring, making a dihedral angle of 4.5(2)°. In **2**, the nitro group is twisted by 15.8(6)° with the salicylidene ring plane. All those metrical parameters are in accordance with previously reported structural data for related tetradentate ferrocenoyl enaminone ligands and their unsymmetrical Schiff base derivatives.[19,35a,41,42,47]

Bimetallic complex 3: Compound **3** consists of a ferrocenyl moiety linked to a Ni(II)-centered unsymmetrical macroacyclic Schiff-base entity (Figure 2 bottom). The N_2O_2-tetradentate binding mode leads to the formation of a six-, five-, six-membered chelate ring arrangement around the central nickel ion, with O–Ni–N bite angles of ~95° (Table 1). The nitrogen and oxygen atoms occupy mutually *trans* dispositions with diagonal O–Ni–N angles deviating somewhat from linearity (5–8°, Table 1). Thus, the nickel(II) atom adopts a slightly distorted square planar geometry with τ_4 index values of 0.103 for **3A** and 0.079 for **3B** ($\tau_4 = 0$ for a perfect square planar geometry).[48] The Ni(N_2O_2) core is part of a bowed chelate Schiff base scaffold with angles of 166.34(15)° and 170.15(15)° between the two central carbon atoms of the 6-membered chelate rings, C(12) and C(22), and the Ni atom. This curvature is accounted for by a more rigid 1,2-cyclohexandiyl spacer as related species of such unsymmetrically substituted Schiff base ligand containing the more flexible ethylene bridge are essentially planar.[25b,49]

The bond lengths and angles in the first coordination sphere of the centered nickel ions (Table 1) are very similar to those measured for related Ni(II) acyclic unsymmetrical Schiff-base complexes.[24c,42a,49,50] The two fused six-membered hetero-metallacycles having O–C, C–C and C–N bond falling between single and double bond lengths and bond angles of sp^2 hybridized atoms (Table S1, Supporting Information),[46] are essentially co-planar. Additionally, both the substituted cyclo-pentadienyl ring of the donor ferrocenyl fragment and the electron withdrawing nitro group are also almost coplanar with the fused heterometallacycle framework, making dihedral angles of 9.7(4)/4.47(13)° and 14.5(7)/4.07(15)° in **3A** and **3B**, respectively, suggesting a significant delocalization of the electron density throughout the entire π-conjugated system.

Electrochemical properties

The redox behavior of the new compounds **2**–**6** was investigated using cyclic voltammetry (CV) in DMF containing 0.1 M [*n*-Bu_4N][PF_6] as supporting electrolyte. The CV measurements were performed at room temperature in the +0.1 to +1.0 V *vs.* Ag/AgCl potential range with scan rate of 100 mV s^{-1}. All the five compounds display one electrochemically reversible oxidation process due to the monoelectronic oxidation of the ferrocenyl moiety,[51] with current ratio i_{pa}/i_{pc} equal to unity. Cyclovoltammograms of the bimetallic complexes **3**–**6** are presented in Figure 3. The redox potentials are all shifted toward more anodic values than that of free ferrocene under the same electrochemical conditions (Table 2). This increased difficulty in oxidizing the Fe^{II} center with respect to free

Research Article
doi.org/10.1002/ejic.202200478

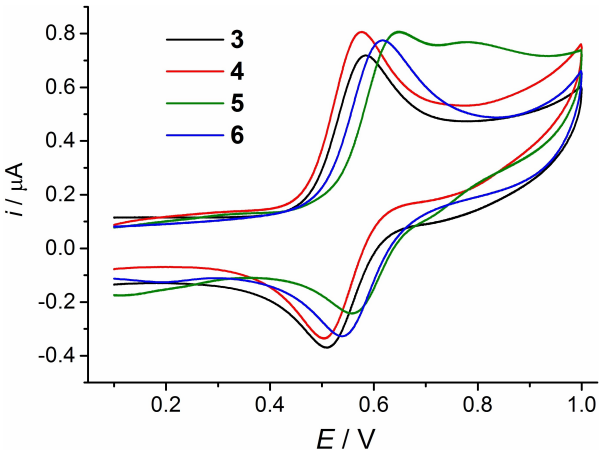

Figure 3. Cyclic voltammograms of complexes **3–6** recorded at a glassy carbon working electrode in DMF containing 0.1 M [*n*-Bu_4N][PF_6] at $T = 298$ K with a sweep rate $v = 0.1$ V s^{-1}, reference electrode Ag/AgCl. The second redox event observed in the Zn^{II} complex **5** could be attributed to an adsorption process.

Table 2. Formal electrode potentials and peak-to-peak separations for the Fe^{II}/Fe^{III} redox processes exhibited by compounds **2–6.**[a]

Compd.	M(II)	$E_{1/2}$ [V]	ΔE_p [mV]
2	–	0.59	78
3	Ni	0.55	75
4	Cu	0.54	70
5	Zn	0.60	88
6	Pd	0.58	78
Cp_2Fe	–	0.40	98

[a] Recorded at a glassy carbon working electrode in DMF containing 0.1 M [*n*-Bu_4N][PF_6] at $T = 298$ K with a sweep rate $v = 100$ mV s^{-1}, reference electrode Ag/AgCl.

ferrocene is due to the electron-withdrawing nature of the side-chain free (for **2**) or metallated (for **3–6**) Schiff-base substituent. The $E_{1/2}$ values measured for **2**, and for **3** and **4** corroborate what we have previously observed with ferrocene-containing diprotonated N_2O_2 macrocycles and their corresponding four-coordinate Ni^{II} and Cu^{II} derivatives, respectively.[25b,42,50b] Interestingly, anodic shifts of 200 and 180 mV observed for the Zn^{II} (**5**) and Pd^{II} (**6**) derivatives, respectively, significantly greater than those found for their counterparts **3** and **4** (Table 2), clearly indicate that these transition-metal ions greatly facilitate the electronic communication between the donor and acceptor parts of the molecule. It is also likely that the Zn^{II} and Pd^{II} centers are playing an electro-attractive effect due to their higher Lewis acidity.[52] Such a behaviour has previously been observed for Pd(II) Schiff base complexes.[42a]

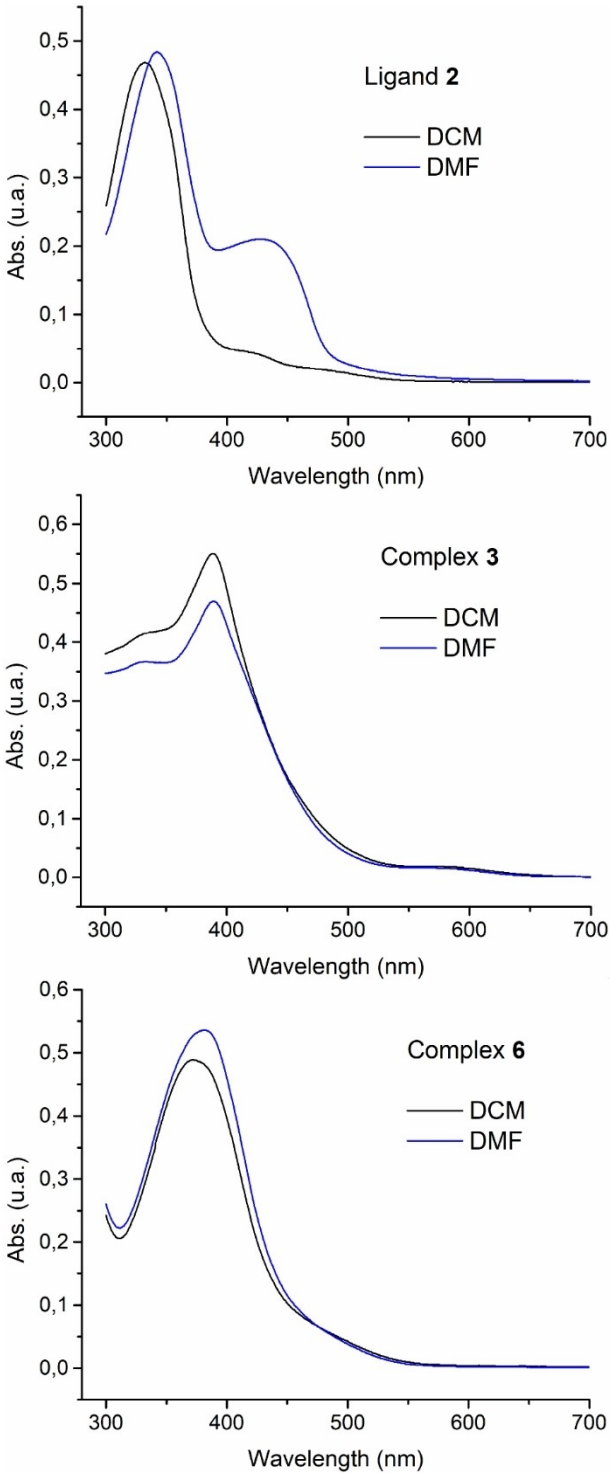

Figure 4. UV/vis spectra of Schiff base proligand **2** (top), complexes **3** (middle) and **6** (bottom) recorded in DCM (black line) and DMF (blue line) solutions.

Electronic Absorption Spectra

The electronic absorption spectra of the chiral metalloligand **2**, and Schiff base complexes **3–6** in the UV/vis region were measured in dichloromethane (DCM, $\varepsilon = 8.90$) and dimethylformamide (DMF, $\varepsilon = 36.7$) (Figure 4 and Figure S19 in Supporting information). The spectral data are reported in Table 3. The higher energy band observed at $\lambda = 342$ nm in the spectrum of **2** is based on π-π* transition due to the imine groups and aromatic rings, while the band of lower energy ($\lambda =$ 428 nm) is associated with charge transfer from the donor

Research Article
doi.org/10.1002/ejic.202200478

Table 3. Experimental UV/vis absorption data for compounds **2–6**.

Compd.	M(II)	λ [nm] (Log ξ) (DCM)	λ [nm] (Log ξ) (DMF)	Solv. Shift [cm^{-1}]
2	–	342 (4.38)	332 (4.37)	+881
		428 (4.02)	423 (3.34)	+276
3	Ni	389 (4.37)	388 (4.44)	+66
4	Cu	370 (4.33)	362 (4.36)	+597
5	Zn	344 (4.45)	346 (4.53)	−168
6	Pd	394 (3.34)	389 (3.44)	+326

ferrocenyl to the acceptor nitro group. By contrast, the experimental spectra of complexes **3–6** are mainly composed of a broad absorption band exhibiting a maximum in the λ_{max} = 344–394 nm region (Table 3), and are mainly influenced by $\pi\rightarrow$ M ligand-to-metal charge transfer (LMCT) and, to a lesser extent, M$\rightarrow\pi^*$ metal-to-ligand charge transfer (MLCT) (see below). All those major features are reproduced on passing from DCM to the polar DMF solvent, but without significant solvatochromic shifts (Table 3).

Quadratic NLO Studies

Second-order polarizabilities β of compounds **1–6** have been measured in dichloromethane solution by using Harmonic Light Scattering (HLS) at 1.91 μm incident wavelength, and the values are reported in Table 4, along with those of a closely related family of non-chiral complexes,[25b,42a] [M{Fc–C(=O)CH=C(4-C_6H_4OH)N–C_2H_4–N=CH–(2-O,5-NO_2–C_6H_3)}] (M = none, **2′**; Ni, **3′**; Cu, **4′**; Zn, **5′**; Pd, **6′**), for which the methyl group and the (1*R*,2*R*)-1,2-cyclohexane-diyl spacer have been substituted for a 4-hydroxyphenyl moiety and 1,2-ethane-diyl linker, respectively. For both series, the relative experimental error does not exceed 10%. However, one must note that measurements for compounds **2′-6′** were performed in the most polar dimethylformamide (DMF) solvent.

The smaller nonlinear response of the half unit precursor **1** as compared to that of the diprotic proligand **2** can be accounted for by the absence of the nitrobenzene moiety, which reinforces the intramolecular charge transfer, responsible for molecular quadratic NLO properties, within the Schiff base derivative. The presence of metal ions tends to increase the β values as compared to those of the free ligand **2**, except for the Zn complex for which the β value is the smallest of the metallic series. This can be understood considering that the electrochemical data indicate that the electronic structure of **5** is essentially similar to that of **2**, since filled d orbitals do not allow electronic communication through empty orbitals. On the other hand, the hyperpolarizability of the palladium complex **6** is found to be much higher than those of its nickel, copper and zinc counterparts **3–5**, respectively (Table 4). Interestingly, the same trend is observed for the non-chiral series **2′-6′**, with a hyperpolarizability order: **5′** < **3′** < **4′** ≪ **6′** (Table 4). Such higher β values observed for Schiff base complexes of second row transition metals,[42a] could be attributed to higher electronic density and participation of the metal orbitals which favors the electronic interaction between the electro-releasing and electro-withdrawing groups throughout the entire [Pd(N_2O_2)] coordination core.[53] One can also notice that the nonlinear responses found for the chiral series **2–6** reported in this work are weaker, almost two-fold smaller for **2** *vs.* **2′** and **6** *vs.* **6′**, than those we previously determined for the non-chiral compounds **2′-6′** (Table 4). This suggests that introducing a chiral backbone is not a sufficient tool to increase the NLO properties, at least in solution. By contrast, the presence of the 4-hydroxyphenyl group enable to generate supramolecular architectures through hydrogen bonds, could favor a better organization of the chromophoric entities, thus optimizing the NLO response of Schiff-base complexes.

Table 4. Second-order polarizabilities β of compounds **1–6** and closely related complexes [M{Fc–C(=O)CH=C(4-C_6H_4OH)N–C_2H_4–N=CH–(2-O,5-NO_2–C_6H_3)}] (**2′–6′**) as measured by HLS at 1.9 μm.

Compound	M(II)	Concentration ($mol\cdot L^{-1}$)	β (10^{-30} esu)	Ref.
1[a]	–	1.12 10^{-3}	55	This work
2[a]	–	5.71 10^{-3}	120	This work
2′[b]	–	1.0 10^{-2}	200	[42a]
3[a]	Ni	2.35 10^{-3}	190	This work
3′[b]	Ni	1.0 10^{-2}	220	[42a]
4[a]	Cu	4.61 10^{-3}	205	This work
4′[b]	Cu	1.0 10^{-2}	250	[25b]
5[a]	Zn	7.29 10^{-3}	130	This work
5′[a]	Zn	1.0 10^{-2}	140	[25b]
6[a]	Pd	4.55 10^{-3}	460	This work
6′[b]	Pd	1.0 10^{-2}	970	[42a]

[a] In dichloromethane (DCM). [b] In dimethylformamide (DMF).

Computational investigations

Density functional theory (DFT) calculations at the PBE0/TZ2P level were performed to optimize the geometries of compounds **2–6** (see Exp. Sect., Computational Details). The five optimized structures are shown in Figure 5. Selected computed data are provided in Table 5. The optimized geometries of **2** and **3** are in good agreement with their X-ray structures (compare Figure 2 with Figure 4 and Table 1 with Table 5). The

Table 5. Selected computed data for complexes **3–6**. Distances in Å and angles in °.

	3	**4**	**5**	**6**
HOMO-LUMO gap (eV)	3.87	–	4.02	3.92
Ionization energy (eV)	6.22	6.21	6.86	6.18
M(1)–O(1)	1.827	1.886	1.931	1.983
M(1)–O(2)	1.850	1.919	1.928	2.003
M(1)–N(1)	1.868	1.949	2.006	1.986
M(1)–N(2)	1.840	1.932	2.022	1.952
Fe–$C(Cp)_{av}$	2.032	2.031	2.032	2.031
O(1)–M(1)–N(2)	175.8	174.5	151.2	179.7
O(2)–M(1)–N(1)	173.4	166.1	146.4	174.0
Planarity index τ_4[47]	0.08	0.14	0.44	0.04
O(1)–M(1)–O(2)	84.5	89.2	105.5	87.0
O(1)–M(1)–N(1)	96.0	95.2	93.6	95.7
O(2)–M(1)–N(2)	93.6	92.4	92.9	93.2
N(1)–M(1)–N(2)	86.3	84.4	82.1	84.1
Σ four bond angles	360.4	361.2	374.1	360.0

Research Article
doi.org/10.1002/ejic.202200478

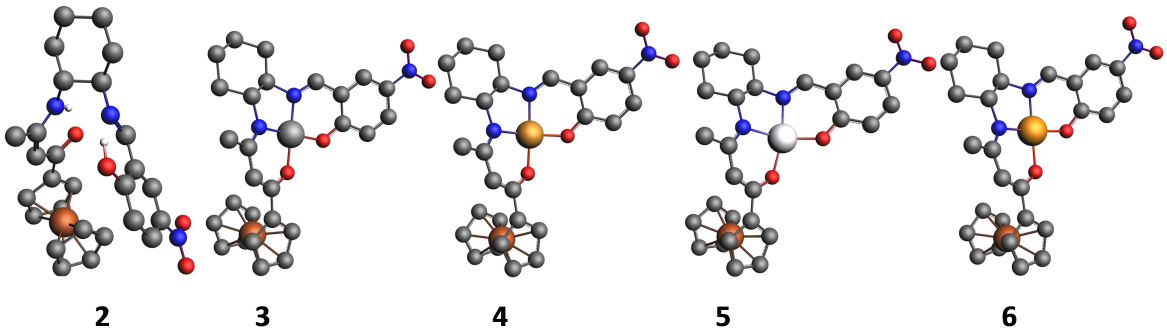

Figure 5. DFT-optimized geometries of compounds **2**–**6**. Hydrogens, except those involved in hydrogen bonding interaction in **2**, are omitted for clarity.

N(1)–H···O(1) and O(2)–H···N(2) hydrogen bonds are confirmed by DFT, with H···O(1) and H···N(2) distances of 1.761 Å and 1.663 Å, respectively. Complexes **3**–**6** adopt a similar shape, with a ferrocenyl unit somewhat more perpendicular to the M coordination (approximate) plane than in the X-ray structure of **3**, presumably because of the packing forces in the later. The ferrocenyl structure is not affected by the nature of M, as exemplified by the averaged Fe–C(Cp) distances which are, in the four complexes, almost equal to that computed for the proligand **2** (2.033 Å). The sum of the bond angles around M and the values of the planarity index τ_4 (Table 5) are consistent with nearly ideal square-planar coordination for the d^8 16-electron complexes **3** and **6**. Filling the antibonding orbital of large $3d_{x2\text{-}y2}$ character with one (**4**) and two (**5**) electrons results in a small (**3**) and significant (**5**) tetrahedral distortion, as indicated by the τ_4 value of 0.14 and 0.44, respectively ($\tau_4 = 1$ in the case of a perfect tetrahedron[48]).

The frontier orbital diagrams of the closed-shell compounds **2**, **3**, **5** and **6** are shown in Figure 6. The HOMO of the proligand **2** is mainly located on Fe (63%), with some enaminone participation. Unsurprisingly, its LUMO is of major π*(nitro) nature, with some delocalization of the C_6 ring. It turns out that the frontier orbitals of complexes **3**–**6** resemble that of **2** (Figure 6). In fact, in all these complexes, the M levels are situated below the three orbitals of 3d(Fe) parentage. This is also the case for the spinorbital containing the Cu^{II} unpaired electron in **4** (no shown in Figure 6). As a consequence, the oxidation of compounds **2**–**6** is found to occur at the Fe^{II} center, in line with the electrochemical experiments. As shown in Figure S20 (Supporting Information), there is a good linear correlation between the computed ionization energies of **2**–**5** (Table 5) and their experimental $E_{1/2}$ values (Table 2). The (moderate) discrepancy afforded by the Pd^{II} complex **6** might be tentatively attributed to a different behavior of this heavy atom species with the solvent and/or electrolyte.

TD-DFT calculations were also performed on compounds **2**–**6** for indexing their absorption bands. The corresponding simulated spectra a shown in Figure S21 (Supporting Information). The agreement with experiment is only qualitative, but the shape of the spectra is satisfyingly reproduced. In the case of **2**, the more intense high-energy band is of LLCT character and in the case of the other complexes it is mixed with some MLCT character. The second more intense band (or shoulder) of **2** is of large ferrocenyl-to-nitro charge transfer nature. The experimentally observed increase of intensity of this band in DMF is reproduced when the effect of this solvent is introduced in the calculations (Figure S22). Its charge transfer nature remains unchanged. In the complexes **3**–**6** this band is substantially weaker and gets M-to-ligand character.

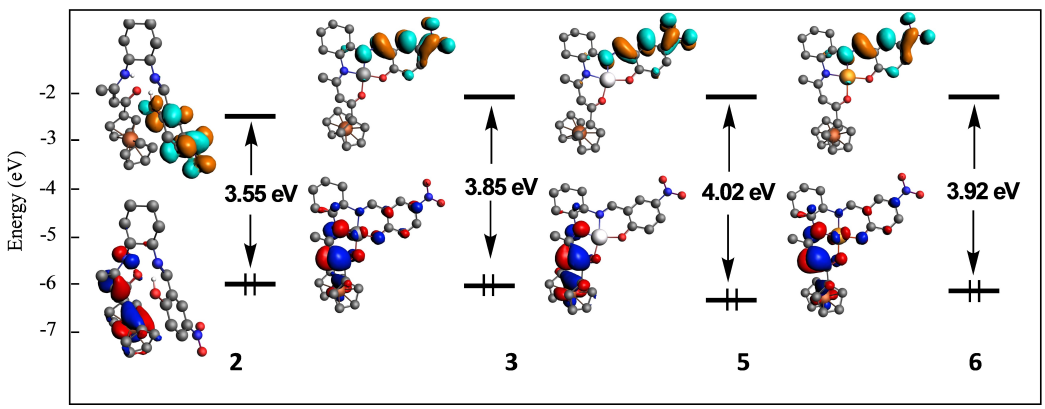

Figure 6. The Kohn-Sham frontier orbitals of **2**, **3**, **5** and **6**.

Research Article
doi.org/10.1002/ejic.202200478

Conclusions

In this contribution, we have synthesized and fully characterized a series of five chiral N_2O_2-tetradentate Schiff base metalloligand and complexes, using the enantiomerically pure (1*R*,2*R*)-1,2-diaminocyclohexane spacer as the chiral source. The neutral bimetallic Ni(II), Cu(II), Zn(II) and Pd(II) complexes of the ferrocene-containing unsymmetrically-substituted Schiff base ligand form D-π-A push-pull chromophores. Their electrochemical, linear, and second-order nonlinear optical properties have been thoroughly investigated. X-ray diffraction study of the metalloligand and Ni(II) complex showed that the two compounds crystallize in the same orthorhombic non-centrosymmetric space group $P2_12_12_1$, with two (*R*,*R*) chiral carbon atoms in their structure. In the nickel(II) complex, the central metal ion adopts a four-coordinate square planar geometry with delocalization of bonding electron density throughout the $[M^{II}(N_2O_2)]$ coordination plane. DFT calculations have been performed to assess the structures of all the complexes. Their electronic structures are strongly related, with the highest occupied and lowest vacant orbitals being centered on the ferrocenyl and the nitro salicyldenyl molecular end, respectively. These results are supported by NLO data, and confirm the importance of an intramolecular charge transfer within the ligand to optimize the quadratic nonlinear response of these complexes. Next step will explore the organization of the NLO-phores in polymeric films.

Experimental Section

General considerations: All manipulations were carried out under a dinitrogen atmosphere using standard Schlenk techniques. The solvents were dried and distilled according to standard procedures.[54] Pure enantiomerically (1*R*,2*R*)-(−)-1,2-diaminocyclohexane, 2-hydroxy-5-nitrobenzaldehyde, nickel(II) acetate tetrahydrate, copper(II) acetate monohydrate, zinc(II) acetate dihydrate and palladium(II) acetate were purchased from Aldrich and used without further purification. The chiral half-unit (1*R*,2*R*)Fc–C(=O)CH=C(CH_3)NH-*c*-C_6H_{10}–NH_2 (**1**) was synthesized according to literature procedures.[36] Solid-state FT-IR spectra were recorded on a Perkin-Elmer Model 1600 FT-IR spectrophotometer with KBr disks in the 4000 to 400 cm^{-1} range. Electronic spectra were obtained with a SHIMADZU UV-1800 spectrophotometer. NMR spectra were obtained at 298 K on a Bruker Avance III 400 spectrometer (^{1}H NMR at 400.13 MHz and ^{13}C NMR at 100.6 MHz). All NMR spectra are reported in parts per million (δ, ppm) relative to tetramethylsilane (Me_4Si), with the residual solvent proton and carbon resonances used as internal standards. Coupling constants (*J*) are reported in Hertz (Hz), and integrations are reported as number of protons. The following abbreviations are used to describe peak patterns: s = singlet, d = doublet, t = triplet, m = multiplet, br = broad. ^{1}H and ^{13}C NMR chemical shift assignments are supported by data obtained from ^{1}H-^{1}H COSY, ^{1}H-^{13}C HMQC, and ^{1}H-^{13}C HMBC NMR experiments, and are given according to the numbering scheme depicted in Figure 7. High resolution electrospray ionization mass spectra (ESI-MS) were obtained at the Centre Regional de Mesures Physiques de l'Ouest (CRMPO, Université de Rennes1, France) with a Bruker MAXI 4G spectrometer. Elemental analyses were conducted on a Thermo-Finnigan Flash EA 1112 CHNS/O analyzer by the Microanalytical Service of the CRMPO. Cyclic voltammetry (CV) measurements were performed with a CH instruments/model Ch604E potentiostat, using a standard three-electrode setup with a glassy carbon working electrode, platinum wire auxiliary electrode, and Ag/AgCl as the reference electrode. Dimethylformamide (DMF) solutions were 1.0 mM in the compound under study and 0.1 M in the supporting electrolyte [*n*-Bu_4N][PF_6] with voltage scan rate of 100 mV s^{-1}. Ferrocene was added as an internal standard at the end of each experiment.

Synthesis of (1*R*,2*R*)-Fc–C(=O)CH=C(CH_3)NH-*c*-C_6H_{10}N=CH–(2-OH,5–NO_2–C_6H_3) (2): To a Schlenk flask equipped with a condenser and containing a stirred solution of 2-hydroxy-5-nitrobenzaldehyde (219 mg, 1.31 mmol) in ethanol (7 mL) was added dropwise a solution of **1** (400 mg, 1.09 mmol) in 15 mL of ethanol. After completion of the addition, the reaction medium was refluxed for 2 h. After cooling to room temp., the Schlenk tube was stored at −15 °C for 5 days. The red crystalline precipitate was collected by filtration, washed with cold methanol, diethyl ether and pentane (2×5 mL), and dried under vacuum. Yield: 490 mg, 87 %. A single crystal suitable for X-ray diffraction study was selected from this crop. ^{1}H NMR (400 MHz, [d_6]DMSO): δ = 1.54 (m, 2H; H9$_a$ + H-10$_a$), 1.62 (m, 2H; H-10$_{b+H}$-11$_a$), 1.88 (m, 2H; H-9$_{b+H}$-12$_a$), 2.03 (s, 3H; CH_3), 2.13 (m, 1H; H-12$_b$), 3.54 (m, 1H; H-8), 3.85 (m, 1H; H-7), 4.03 (s, 5H; C_5H_5), 4.38 (s, 2H; H$_\beta$ C_5H_4), 4.67 (s, 2H; H$_\alpha$ C_5H_4), 5.24 (s, 1H; CH=C), 6.78 (d, $^3J_{H,H}$ = 2.3 Hz, 1H; H-3), 8.03 (dd, $^3J_{H,H}$ = 2.3 Hz, $^4J_{H,H}$ = 0.6 Hz, 1H; H-4), 8.35 (d, $^4J_{H,H}$ = 0.6 Hz, 1H; H-6), 8.73 (s, 1H; N=CH), 10.86 (d, $^3J_{H,H}$ = 2.5 Hz, 1H; NH), 14.40 ppm (br s, 1H; OH); ^{13}C{^{1}H} NMR (101 MHz, [d_6]DMSO): δ = 19.1 (CH_3), 23.5 (C-10), 23.9 (C-11), 31.2 (C-9), 32.6 (C-12), 55.2 (C-8), 67.9 (C$_\alpha$ C_5H_4), 68.9 (C-7), 69.2 (C_5H_5), 70.2 (C$_\beta$ C_5H_4), 82.6 (C$_{ipso}$ C_5H_4), 92.6 (*C*H=C), 114.9 (C-1), 120.9 (C-3), 128.8 (C-4), 130.6 (C-6), 135.8 (C-5), 161.2 (CH–*C*), 165.6 (N=CH), 173.5 (C-2), 190.4 ppm (C=O); IR (KBr): $\bar{\upsilon}$ = 3432 (w) (O–H), 3260 (w) (N–H), 3095 (w), 3064 (w) (C–H arom), 2934 (m), 2857 (m) (C–H aliph), 1602 (vs) (C=O), 1564 (s), 1556 (s) (C=C) and/or (C=N), 1521 (s) asym (N=O), 1302 (vs) sym (N=O), 728 cm^{-1} (m) (C–H); HRMS (ESI): *m/z* calcd for $C_{27}H_{29}N_3O_4{}^{56}Fe^+$: 515.1502 $[M]^+$; found: 515.1508; *m/z* calcd for $C_{27}H_{29}N_3O_4Na{}^{56}Fe^+$: 538.14052 $[M+Na]^+$; found: 538.14.

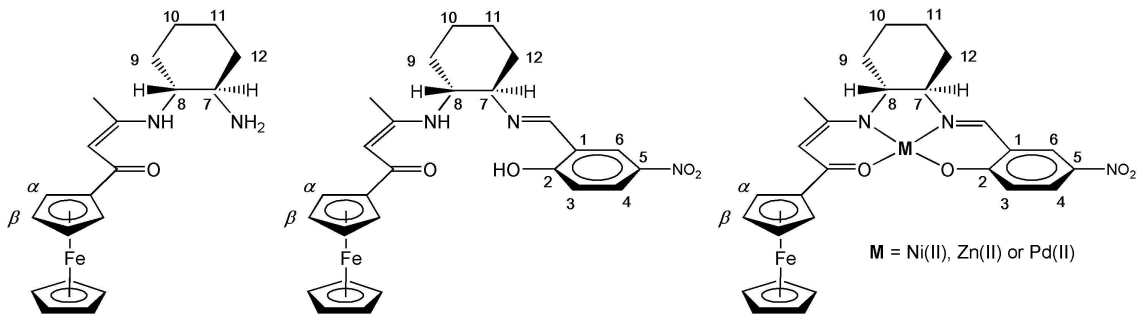

Figure 7. Labelling scheme used for NMR assignments.

Elemental analysis Calcd (%) for $C_{27}H_{29}FeN_3O_4$: C 62.92, H 5.67, N 8.15; found: C 62.61, H 5.62, N 7.92.

Synthesis of [Ni{(1*R*,2*R*)-Fc–C(=O)CH=C(CH$_3$)N-*c*-C$_6$H$_{10}$–N=CH-(2–O,5–NO$_2$–C$_6$H$_3$)}] (3): To a Schlenk tube containing a stirred solution of **1** (300 mg, 0.82 mmol) in ethanol (15 mL) was added dropwise 2-hydroxy-5-nitrobenzaldehyde (140 mg, 0.82 mmol) in ethanol (10 mL) and the stirring was continued for 5 min. Then, a solution of nickel(II) acetate tetrahydrate (208 mg, 0.82 mmol) in ethanol (5 mL) was added and the reaction medium was refluxed for 2 h, giving a brown microcrystalline precipitate. Upon cooling to room temp., the solid material was collected by filtration, washed with cold methanol and diethyl ether (2×5 mL), and dried under vacuum. Yield: 375 mg, 80 %. X-ray quality crystals were obtained by slow diffusion of diethyl ether into a solution of complex **3** in a 1:1 mixture of dimethylformamide and ethanol. ^{1}H NMR (400 MHz, [d$_6$]DMSO): δ = 1.17 (m, 1H; H-10$_a$), 1.20 (m, 1H; H-9$_a$), 1.26 (m, 1H; H-11$_a$), 1.44 (m, 1H; H-10$_b$), 1.77 (m, 1H; H-12$_a$), 1.85 (m, 1H; H-11$_b$), 2.20 (s, 3H; CH$_3$), 2.43 (m, 1H; H-12$_b$), 2.49 (m, 1H; H-9$_b$), 3.07 (m, 1H; H-8), 3.79 (m, 1H; H-7), 4.23 (s, 5H; C$_5$H$_5$), 4.37 (s, 2H; H$_\beta$ C$_5$H$_4$), 4.60 (s, 1H; H$_\alpha$ C$_5$H$_4$), 4.65 (s, 1H; H$_{\alpha'}$ C$_5$H$_4$), 5.47 (s, 1H; CH=C), 6.71 (d, $^3J_{H,H}$ = 2.3 Hz, 1H; H-3), 7.82 (bs, 1H; H-6), 7.96 (dd, $^3J_{H,H}$ = 2.3 Hz, $^4J_{H,H}$ = 0.7 Hz, 1H; H-4), 8.49 ppm (d, $^4J_{H,H}$ = 0.7 Hz, 1H; N=CH); ^{13}C{^{1}H} NMR (101 MHz, [d$_6$]DMSO): δ = 23.2 (CH$_3$), 23.7 (C-10), 24.9 (C-11), 27.3 (C-9), 32.5 (C-12), 66.5 (C-8), 67.5 (C$_\alpha$ C$_5$H$_4$), 67.9 (C$_{\alpha'}$ C$_5$H$_4$), 69.5 (C$_5$H$_5$), 69.6 (C$_\beta$ C$_5$H$_4$), 73.7 (C-7), 80.4 (C$_{ipso}$ C$_5$H$_4$), 99.5 (*C*H=C), 120.3 (C-3), 120.7 (C-1), 127.5 (C-4), 131.0 (C-6), 135.0 (C-5), 157.0 (N=CH), 168.9 (CH–*C*), 169.8 (C-2), 174.0 ppm (C=O); IR (KBr): $\bar{\upsilon}$ = 3090 (vw), 3055 (vw) (C–H arom), 2927 (w), 2857 (w) (C–H aliph), 1601 (m) (C=O), 1574 (m), 1572 (m) (C=C) and/or (C=N), 1506 (s) asym (N=O), 1321 (vs) sym (N=O), 733 (w) (C–H), 577 (w) (Ni–O), 490 cm^{-1} (w) (Ni–N); HRMS (ESI): *m/z* calcd for $C_{27}H_{27}N_3O_4{}^{56}Fe^{58}Ni^+$: 571.06989 [M]$^+$; found: 571.0698; *m/z* calcd for $C_{27}H_{27}N_3O_4Na^{56}Fe^{58}Ni^+$: 594.06021 [M + Na]$^+$; found: 594.0587; Elemental analysis Calcd (%) for $C_{27}H_{27}FeN_3NiO_4$: C 56.69, H 4.76, N 7.35; found: C 56.48, H 4.70, N, 7.02.

Synthesis of [Cu{(1*R*,2*R*)-Fc–C(=O)CH=C(CH$_3$)N-*c*-C$_6$H$_{10}$–N=CH-(2–O,5–NO$_2$–C$_6$H$_3$)}] (4): The synthesis of this light brown microcrystalline complex was carried out following a similar procedure to that described above for complex **3**, using in this case: **1** (300 mg, 0.82 mmol), 2-hydroxy-5-nitrobenzaldehyde (140 mg, 0.82 mmol), and copper(II) acetate monohydrate (165 mg, 0.826 mmol). Yield: 385 mg, 82 %. IR (KBr): $\bar{\upsilon}$ = 3089 (vw), 3060 (vw) (C–H arom), 2926 (w), 2858 (w) (C–H aliph), 1639 (m) (C=O), 1601 (m), 1572 (m) (C=C) and/or (C=N), 1497 (s) asym (N=O), 1319 (vs) sym (N=O), 723 (w) (C–H), 541 (w) (Cu–O), 426 cm^{-1} (w) (Cu–N); HRMS (ESI): *m/z* calcd for $C_{27}H_{27}N_3O_4{}^{56}Fe^{63}Cu^+$: 576.06415 [M]$^+$; found: 576.0640; Elemental analysis Calcd (%) for $C_{27}H_{27}CuFeN_3O_4$: C 56.21, H 4.72, N 7.28; found: C 56.12, H 4.70, N, 7.10.

Synthesis of [Zn{(1*R*,2*R*)-Fc–C(=O)CH=C(CH$_3$)N-*c*-C$_6$H$_{10}$–N=CH-(2–O,5–NO$_2$–C$_6$H$_3$)}] (5): The synthesis of this light orange microcrystalline complex was carried out following a similar procedure to that described above for complex **3**, using in this case: **1** (300 mg, 0.82 mmol), 2-hydroxy-5-nitrobenzaldehyde (140 mg, 0.82 mmol), 1.0 mL triethylamine before addition of zinc(II) acetate dihydrate (182 mg, 0.82 mmol). In the present case, the reaction time was increased to 5 h. Yield: 350 mg, 74 %. ^{1}H NMR (400 MHz, [d$_6$]DMSO): δ = 0.92 (m, 1H; H-10$_a$), 1.24 (m, 1H; H-9$_a$), 1.37 (m, 1H; H-11$_a$), 1.42 (m, 1H; H-10$_b$), 1.65 (m, 1H; H-11$_b$), 1.72 (m, 1H; H-12$_a$), 2.10 (m, 2H; H-9$_b$ + H-12$_b$), 2.21 (s, 3H; CH$_3$), 3.55 (m, 1H; H-8), 3.72 (m, 1H; H-7), 3.93 (s, 5H; C$_5$H$_5$), 4.36 (s, 2H; H$_\beta$ C$_5$H$_4$), 4.61 (s, 1H; H$_\alpha$ C$_5$H$_4$), 4.67 (s, 1H; H$_{\alpha'}$ C$_5$H$_4$), 5.26 (s, 1H; CH=C), 6.83 (d, $^3J_{H,H}$ = 2.2 Hz, 1H; H-3), 8.10 (dd, $^3J_{H,H}$ = 2.2 Hz, $^4J_{H,H}$ = 0.7 Hz, 1H; H-4), 8.37 (bs, 1H; H-6), 8.74 ppm (s, 1H; N=CH); ^{13}C{^{1}H} NMR (101 MHz, [d$_6$]DMSO): δ = 19.1 (CH$_3$), 23.4 (C-10), 24.3 (C-11), 32.1 (C-9), 33.0 (C-12), 55.4 (C-7), 67.7 (C$_\alpha$ C$_5$H$_4$), 68.0 (C$_{\alpha'}$ C$_5$H$_4$), 69.1 (C$_5$H$_5$), 70.1 (C$_\beta$ C$_5$H$_4$), 70.2 (C$_{\beta'}$ C$_5$H$_4$), 73.9 (C-8), 82.5 (C$_{ipso}$ C$_5$H$_4$), 92.7 (*C*H=C), 116.8 (C-1), 122.9 (C-3), 129.6 (C-4), 134.0 (C-6), 135.8 (C-5), 161.4 (CH–*C*), 171.8 (N=CH), 174.2 (C-2), 190.5 ppm (C=O); IR (KBr): $\bar{\upsilon}$ = 3093 (w), 3061 (w) (C–H arom), 2933 (m), 2854 (m) (C–H aliph), 1616 (vs) (C=O), 1603 (vs), 1551 (vs) (C=C) and/or (C=N), 1496 (s) asym (N=O), 1316 (vs) sym (N=O), 715 (m) (C–H), 541 (w) (Zn–N), 423 cm^{-1} (w) (Zn–O); HRMS (ESI): *m/z* calcd for $C_{27}H_{27}N_3O_4{}^{56}Fe^{64}Zn^+$: 577.06369 [M]$^+$; found: 577.0641; *m/z* calcd for $C_{27}H_{27}N_3O_4Na^{56}Fe^{64}Zn^+$: 600.05401 [M + Na]$^+$; found: 600.0533; Elemental analysis Calcd (%) for $C_{27}H_{27}FeN_3O_4Zn$: C 56.03, H 4.70, N, 7.26; found: C 55.61, H 4.95, N 7.06.

Synthesis of [Pd{(1*R*,2*R*)-Fc–C(=O)CH=C(CH$_3$)N-*c*-C$_6$H$_{10}$–N=CH-(2–O,5–NO$_2$–C$_6$H$_3$)}] (6): The synthesis of this brown microcrystalline complex was carried out following a similar procedure to that described above for complex **3**, using in this case: **1** (300 mg, 0.82 mmol), 2-hydroxy-5-nitrobenzaldehyde (140 mg, 0.82 mmol), and palladium(II) acetate (184 mg, 0.826 mmol). Yield: 435 mg, 86 %. ^{1}H NMR (400 MHz, [d$_6$]DMSO): δ = 1.36 (m, 1H; H-10$_a$), 1.47 (m, 1H; H-9$_a$), 1.65 (m, 1H; H-11$_a$), 1.83 (m, 2H; H-10$_b$ + H-12$_a$), 1.90 (m, 1H; H-11$_b$), 2.32 (s, 3H; CH$_3$), 2.67 (m, 1H; H-12$_b$), 2.74 (m, 1H; H-9$_b$), 3.60 (m, 1H; H-8), 3.91 (m, 1H; H-7), 4.22 (s, 5H; C$_5$H$_5$), 4.42 (bs, 2H; H$_\beta$ C$_5$H$_4$), 4.74 (s, 1H; H$_\alpha$ C$_5$H$_4$), 4.76 (s, 1H; H$_{\alpha'}$ C$_5$H$_4$), 5.44 (s, 1H; CH=C), 6.90 (d, $^3J_{H,H}$ = 2.3 Hz, 1H; H-3), 8.08 (dd, $^3J_{H,H}$ = 2.3 Hz, $^4J_{H,H}$ = 0.7 Hz, 1H; H-4), 8.22 (bs, 1H; H-6), 8.67 ppm (d, $^4J_{H,H}$ = 0.7 Hz, 1H; N=CH); ^{13}C{^{1}H} NMR (101 MHz, [d$_6$]DMSO): δ = 23.6 (CH$_3$), 23.7 (C-10), 25.1 (C-11), 27.6 (C-9), 32.6 (C-12), 67.9 (C$_\alpha$ C$_5$H$_4$), 69.5 (C$_5$H$_5$), 69.6 (C-8), 69.7 (C$_\beta$ C$_5$H$_4$), 76.4 (C-7), 81.2 (C$_{ipso}$ C$_5$H$_4$), 98.8 (*C*H=C), 121.0 (C-3), 121.1 (C-1), 128.3 (C-4), 133.2 (C-6), 135.0 (C-5), 155.6 (N=CH), 165.8 (CH–*C*), 170.2 (C-2), 174.3 ppm (C=O); IR (KBr): $\bar{\upsilon}$ = 3092 (w), 3036 (vw) (C–H arom), 2929 (w), 2856 (w) (C–H aliph), 1603 (s), (C=O), 1562 (m), 1550 (s) (C=C) and/or (C=N), 1499 (s) asym (N=O), 1316 (vs) sym (N=O), 726 (w) (C–H), 540 (w) (Pd–O), 494 cm^{-1} (w) (Pd–N); HRMS (ESI): *m/z* calcd for $C_{27}H_{27}N_3O_4{}^{56}Fe^{106}Pd^+$: 619.03802 [M]$^+$; found: 619.0390; *m/z* calcd for $C_{27}H_{27}N_3O_4Na^{56}Fe^{106}Pd^+$: 642.02834 [M + Na]$^+$; found: 642.0277; Elemental analysis Calcd (%) for $C_{27}H_{27}FeN_3O_4Pd$: C 52.32, H 4.39, N 6.78; found: C 52.23, H 4.35, N 6.60.

X-ray Crystal Structure Determinations: A well-shaped single crystal of each compound **2** and **3**, was mounted on top of glass fibers in a random orientation. Diffraction data were collected at 296(2) K on a Bruker D8 QUEST diffractometer equipped with a bidimensional CMOS Photon100 detector, using graphite monochromated Mo-Kα radiation (λ = 0.71073 Å). The diffraction frames were integrated using the APEX2 package,[55] and were corrected for absorptions with SADABS. The structures were solved by direct methods using the OLEX 2 program.[56] All the structures were then refined with full-matrix least-square methods based on F^2 (SHELXL-97).[57] All non-hydrogen atoms were refined with anisotropic atomic displacement parameters. All hydrogen atoms were included in their calculated positions, assigned fixed isotropic thermal parameters and constrained to ride on their parent atoms. A summary of the details about crystal data, collection parameters and refinement are documented in Table 6, and additional crystallographic details are in the CIF files. ORTEP views were drawn using OLEX2 software.[56]

HLS Measurements: For the second-order NLO measurements of the Schiff-base chromophores **1–6**, Harmonic Light Scattering (HLS)[27] was performed using a 10 Hz repetition-rate nanosecond Nd^{3+}:YAG laser to obtain the first-order hyperpolarizabilities (β). The measurements at a fundamental wavelength of 1.91 μm were carried out with solutions of **1–6** in dichloromethane (see Table 4 for concentrations used). The solvent appears to be transparent at 1.91 μm. A concentrated (10^{-2} M) solution of ethyl violet (its octupolar β value being 170×10^{-30} esu at 1.91 μm) was used as external reference.[58] By using a wavelength of 1.91 μm, the harmonics at 955 nm remains far from any resonance of the

Research Article
doi.org/10.1002/ejic.202200478

Table 6. Crystallographic data, details of data collection and structure refinement parameters for compounds **2** and **3**.

	2	**3**
Empirical Formula	$C_{27}H_{29}FeN_3O_4$	$C_{27}H_{27}FeN_3NiO_4$
Formula mass, g mol^{-1}	515.38	572.07
Collection T, K	296(2)	296(2)
crystal system	Orthorhombic	Orthorhombic
space group	$P2_12_12_1$	$P2_12_12_1$
a (Å)	10.7362(11)	21.6071(5)
b (Å)	10.9057(11)	9.3086(2)
c (Å)	21.7366(19)	24.5199(4)
V (Å^3)	2545.0(4)	4931.73(18)
Z	4	8
D_{calcd} (g cm^{-3})	1.345	1.541
Crystal size (mm)	0.281×0.19×0.178	0.327×0.134×0.116
F(000)	1080	2368
abs coeff (mm^{-1})	0.630	1.391
θ range (°)	2.089 to 26.396	2.340 to 26.414
range h,k,l	−13/13, −13/13, −27/27	−27/27, −11/11, −30/30
No. total refl.	37942	158337
No. unique refl.	5216	10132
Comp. θ_{max} (%)	99.8	99.9
Max/min transmission	0.9481/0.8574	0.6493/0.4928
Data/Restraints/Parameters	5216/0/318	10132/0/651
Final R	R_1 = 0.0356	R_1 = 0.0330
[$I > 2\sigma(I)$]	wR_2 = 0.0808	wR_2 = 0.0664
R indices (all data)	R_1 = 0.0504	R_1 = 0.0543
	wR_2 = 0.0881	wR_2 = 0.0746
Goodness of fit/F^2	1.061	1.039
Largest diff. Peak/hole (eÅ^{-3})	0.212/−0.157	0.318/−0.226

molecules, then preventing from the contribution of possible two-photon fluorescence emission to the HLS signal. We verified the absence of any wide-band two-photon fluorescence by checking that no HLS signal could be detected for wavelengths other than 955 nm. The experimental setup and details of data analysis have been described previously.[42b]

Computational details: DFT calculations were carried out using the ADF2017 package,[59,60] incorporating the relativistic scalar corrections via the ZORA Hamiltonian,[61] and employing the PBE0 functional[62,63] and the TZ2P basis set,[64] together with Grimme's empirical DFT-D3 corrections for dispersion forces.[65] The optimized geometries (in vacuum) were characterized as true minima on the potential energy surface using vibrational frequency calculations (no imaginary values). The UV-vis transitions were calculated by means of TD-DFT calculations on the optimized geometries, at the same level of theory. In the case of compound **2**, additional TD-DFT calculations including DMF solvent effect through the COSMO model[66,67] were also performed (see Figure S22, Supporting Information). The graphical SWizard program was used for simulating UV-vis spectra.[68,69]

Deposition Numbers 2189540 (for **2**) and 2189541 (for **3**) contain the supplementary crystallographic data for this paper. These data are provided free of charge by the joint Cambridge Crystallographic Data Centre and Fachinformationszentrum Karlsruhe Access Structures service www.ccdc.cam.ac.uk/structures.

Acknowledgements

We thank P. Jehan (CRMPO, Rennes) for helpful assistance with HRMS measurements. This research was performed as part of the Chilean-French International Research Project "IRP-CoopIC". Financial support from the Fondo Nacional de Desarrollo Científico y Tecnológico (FONDECYT), Chile (grant 1090310) and FONDEQUIP EQM130154 and EQM120095], the Vicerrectoría de Investigación y Estudios Avanzados, Pontificia Universidad Católica de Valparaíso, Chile (VRIEA-PUCV), the Centre National de la Recherche Scientifique (CNRS) and the Université de Rennes 1 is gratefully acknowledged. S.C. thanks VRIEA-PUCV for a postdoctoral financing.

Conflict of Interest

The authors declare no conflict of interest.

Data Availability Statement

The data that support the findings of this study are available in the supplementary material of this article.

Keywords: Chiral Schiff bases · Density functional calculations · Nonlinear optics · Transition metals · X-ray diffraction

[1] a) J. F. Nye, *Physical Properties of Crystals*, Oxford University Press, Oxford, UK, **1957**; b) M. E. Lines, A. M. Glass, *Principles and Applications of Ferroelectrics and Related Materials*, Oxford University Press, Oxford, UK, **1991**; c) K. M. Ok, E. O. Chi, P. S. Halasyamani, *Chem. Soc. Rev.* **2006**, *35*, 710–717.

[2] a) E. Goovaerts, W. E. Wenseleers, M. H. Garcia, G. H. Cross, in *Handbook of Advanced Electronic and Photonic Materials and Devices*, (Ed.: H. S. Nalwa), Academic Press, San Francisco, **2001**, Vol. 9: *Nonlinear Optical Materials*, Chap. 3, pp. 127–191; b) *Handbook of Optics IV, Fiber Optics & Nonlinear Optics*, 2nd ed., (Eds.: M. Nass, J. M. Enoch, E. W. V. Stryland, W. L. Wolfe), McGraw-Hill, New York, **2001**; c) *Nonlinear Optical Properties of Mater: From Molecules to Condensed Phases*, (Eds.: M. G.

Papadopoulos, A. J. Sadlej, J. Leszczynski), Springer, India, **2006**; d) *Materials for Nonlinear Optics: Chemical Perspectives*, (Eds.: S. R. Marder, J. E. Sohn, G. D. Stucky), ACS Symposium Series 455, American Chemical Society, Washington, DC, **1991**; e) J. Zyss, *Molecular Nonlinear Optics: Materials, Physics and Devices*, Academic Press, Boston, **1994**; f) Special issue: *Optical Nonlinearities in Chemistry,* (Ed.: D. M. Burland), *Chem. Rev.* **1994**, *94*, 1–278.

[3] J. Zyss, J. L. Oudar, *Phys. Rev. A* **1982**, *26*, 2028–2048.

[4] a) *Structure-Property Relationships in Non-Linear Optical Crystals I,* (Eds.: X.-T. Wu, L. Chen), *Structure and Bonding*, Springer, Berlin Heidelberg, Germany, **2012**, Vol. 144; b) *Structure-Property Relationships in Non-Linear Optical Crystals II,* (Eds.: X.-T. Wu, L. Chen), *Structure and Bonding*, Springer, Berlin Heidelberg, Germany, **2012**, Vol. 145.

[5] M. J. Cho, D. H. Choi, P. A. Sullivan, A. J. P. Akelaitis, L. R. Dalton, *Prog. Polym. Sci.* **2008**, *33*, 1013–1058.

[6] T.-D. Kim, J. Luo, Y. Tian, J.-W. Ka, N. M. Tucker, M. Haller, J.-W. Kang, A. K.-Y. Jen, *Macromolecules* **2006**, *39*, 1676–1680.

[7] L. R. Dalton, P. A. Sullivan, D. H. Bale, *Chem. Rev.* **2010**, *110*, 25–55.

[8] S. Prabu, E. David, T. Viswanathan, K. Thirumoorthy, T. Panda, C. Dragonetti, A. Colombo, D. Marinotto, S. Righetto, D. Roberto, N. Palanisami, *Dalton Trans.* **2020**, *49*, 1854–1863.

[9] L. Viau, S. Bidault, O. Maury, S. Brasselet, I. Ledoux, J. Zyss, E. Ishow, K. Nakatani, H. Le Bozec, *J. Am. Chem. Soc.* **2004**, *126*, 8386–8387.

[10] J. Boixel, V. Guerchais, H. Le Bozec, D. Jacquemin, A. Amar, A. Boucekkine, A. Colombo, C. Dragonetti, D. Marinotto, D. Roberto, S. Righetto, R. De Angelis, *J. Am. Chem. Soc.* **2014**, *136*, 5367–5375.

[11] K. Thirupugalmani, S. Karthick, G. Shanmugam, V. Kannan, B. Sridhar, K. Nehru, S. Brahadeeswaran, *Opt. Mater.* **2015**, *49*, 158–170.

[12] a) B. J. Coe, *Coord. Chem. Rev.* **2013**, *257*, 1438–1458; b) O. Maury, H. Le Bozec,in *Molecular Materials,* Eds. D. W. Bruce, D. O'Hare, R. I. Walton, *Metal-Based Quadratic Nonlinear Optical Materials*, John Wiley & Sons, Ltd, Chichester, UK, **2010**, Chapter 1, pp. 1–59; c) M. G. Humphrey, T. Schwich, P. J. West, M. P. Cifuentes, M. Samoc, in *Comprehensive Inorganic Chemistry II,* (Eds.: J. Reedijk, K. Poeppelmeier), *Nonlinear Optical Properties of Coordination and Organometallic Complexes*, Elsevier, Oxford, UK, **2013**, vol. 8, pp. 781–835.

[13] a) A. Colombo, C. Dragonetti, V. Guerchais, D. Roberto, *Coord. Chem. Rev.* **2021**, *446*, 214113; b) A. Colombo, C. Dragonetti, V. Guerchais, C. Hierlinger, E. Zysman-Colman, D. Roberto, *Coord. Chem. Rev.* **2020**, *414*, 213293.

[14] a) R. J. Durand, S. Achelle, F. Robin-Le Guen, E. Caytan, N. Le Poul, A. Barsella, P. Guevara Level, D. Jacquemin, S. Gauthier, *Dalton Trans.* **2021**, *50*, 4623–4633; b) R. J. Durand, S. Achelle, S. Gauthier, N. Cabon, M. Ducamp, S. Kahlal, J.-Y. Saillard, A. Barsella, F. Robin-Le Guen, *Dyes Pigm.* **2018**, *155*, 68–74.

[15] a) G. Di Carlo, M. Pizzotti, S. Righetto, A. Forni, F. Tessore, *Inorg. Chem.* **2020**, *59*, 7561–7570; b) A. Boulmier, A. Vacher, D. Zang, S. Yang, A. Saad, J. Marrot, O. Oms, P. Mialane, I. Ledoux, L. Ruhlmann, D. Lorcy, A. Dolbecq, *Inorg. Chem.* **2018**, *57*, 3742–3752; c) I. González, D. Cortés-Arriagada, P. Dreyse, L. Sanhueza-Vega, I. Ledoux-Rak, D. Andrade, I. Brito, A. Toro-Labbé, M. Soto-Arriaza, S. Caramori, B. Loeb, *Eur. J. Inorg. Chem.* **2015**, 4946–4955.

[16] a) S. Di Bella, A. Colombo, C. Dragonetti, S. Righetto, D. Roberto, *Inorganics* **2018**, *6*, 133; b) S. Di Bella, C. Dragonetti, M. Pizzotti, D. Roberto, F. Tessore, R. Ugo, *Top. Organomet. Chem.* **2010**, *28*, 1–55; c) S. Di Bella, *Chem. Soc. Rev.* **2001**, *30*, 355–366.

[17] P. G. Lacroix, I. Malfant, C. Lepetit, *Coord. Chem. Rev.* **2016**, *308*, 381–394.

[18] E. David, A. Colombo, C. Dragonetti, N. Palanisami, *Chem. Eur. J.* **2021**, *27*, 7124–7137.

[19] a) N. Novoa, T. Roisnel, P. Hamon, S. Kahlal, C. Manzur, H. M. Ngo, I. Ledoux-Rak, J.-Y. Saillard, D. Carrillo, J.-R. Hamon, *Dalton Trans.* **2015**, *44*, 18019–18037; b) N. Novoa, C. Manzur, T. Roisnel, V. Dorcet, N. Cabon, F. Robin-Le Guen, I. Ledoux-Rak, S. Khalal, J.-Y. Saillard, D. Carrillo, J.-R. Hamon, *New J. Chem.* **2019**, *43*, 10468–10481.

[20] C. R. Nayar, R. Ravikumar, *J. Coord. Chem.* **2014**, *67*, 1–16.

[21] S. Kaur, M. Kaur, P. Kaur, K. Clays, K. Singh, *Coord. Chem. Rev.* **2017**, *343*, 185–219.

[22] X. Liu, C. Manzur, N. Novoa, S. Celedon, D. Carrillo, J.-R. Hamon, *Coord. Chem. Rev.* **2018**, *357*, 144–172.

[23] R. Mazzoni, F. Roncaglia, L. Rigamonti, *Crystals* **2021**, *11*, 483.

[24] a) L. Rigamonti, F. Demartin, A. Forni, S. Righetto, A. Pasini, *Inorg. Chem.* **2006**, *45*, 10976–10989; b) J. Gradinaru, A. Forni, V. Druta, F. Tessore, S. Zecchin, S. Quici, N. Garbalau, *Inorg. Chem.* **2007**, *46*, 884–895; c) L. Rigamonti, A. Forni, S. Righetto, A. Pasini, *Dalton Trans.* **2019**, *48*, 11217–11234.

[25] a) S. Celedón, T. Roisnel, V. Artigas, M. Fuentealba, D. Carrillo, I. Ledoux-Rak, J.-R. Hamon, C. Manzur, *New J. Chem.* **2020**, ***44***, 9190–9201; b) S. Celedón, T. Roisnel, D. Carrillo, I. Ledoux-Rak, J.-R. Hamon, C. Manzur, *J. Coord. Chem.* **2020**, *73*, 3079–3094.

[26] a) J. L. Oudar, D. S. Chemla, *J. Chem. Phys.* **1977**, *66*, 2664–2668; b) J. L. Oudar, *J. Chem. Phys.* **1977**, *67*, 446–457; c) J. L. Oudar, H. Le Person, *Opt. Commun.* **1975**, *15*, 258–262.

[27] R. W. Terhune, P. D. Maker, C. M. Savage, *Phys. Rev.* **1965**, *14*, 681–684.

[28] M. Leolukman, P. Paoprasert, Y. Wang, V. Makhija, D. J. McGee, P. Gopalan, *Macromolecules* **2008**, *41*, 4651–4660.

[29] A. N. Rashid, J. R. Deschamps, *J. Mol. Struct.* **2006**, *787*, 216–219.

[30] K. Mohanalingam, M. Nethaji, P. K. Das, *J. Mol. Struct.* **1996**, *378*, 177–188.

[31] Y. Fan, W. You, W. Huang, J.-L. Liu, Y.-N. Wang, *Polyhedron* **2010**, *29*, 1149–1155.

[32] a) G. Lenoble, P. G. Lacroix, J.-C. Daran, S. Di Bella, K. Nakatani, *Inorg. Chem.* **1998**, *37*, 2158–2165; b) F. Averseng, P. G. Lacroix, I. Malfant, F. Dahan, K. Nakatani, *J. Mater. Chem.* **2000**, *10*, 1013–1018.

[33] L. Rigamonti, A. Forni, E. Cariati, G. Malavasi, A. Pasini, *Materials* **2019**, *12*, 3595.

[34] a) S. K. Kurtz, T. T. Perry, *J. Appl. Phys.* **1968**, *39*, 3798–3813; b) J. P. Dougherty, S. K. Kurtz, *J. Appl. Crystallogr.* **1976**, *9*, 145–158.

[35] a) J. Mahrholdt, E. Kovalski, T. Ruffer, V. Vrček, H. Lang, *Eur. J. Inorg. Chem.* **2022**, e202101059; b) Y.-P. Jiao, H.-Y. Shi, W.-Y. Zhou, A.-Q. Jia, Q.-F. Zhang, *J. Organomet. Chem.* **2022**, *957*, 122149.

[36] S. Celedón, P. Hamon, V. Artigas, M. Fuentealba, S. Kahlal, D. Carrillo, J.-Y. Saillard, J.-R. Hamon, C. Manzur, *New J. Chem.* **2022**, *46*, 3948–3960.

[37] a) W. Qin, S. Long, M. Panunzio, S. Biondi, *Molecules* **2013**, *18*, 12264–12289; b) L. Fabbrizzi, *J. Org. Chem.* **2020**, *85*, 12212–12226.

[38] a) I. Buta, S. Shova, S. Iliesa, F. Manea, M. Andruh, O. Costisor, *J. Mol. Struct.* **2022**, *1248*, 131439; b) H. Kargar, M. Fallah-Mehrjardi, R. Behjatmanesh-Ardakani, M. Bahadori, M. Moghadam, M. Ashfaq, K. S. Munawar, M. N. Tahir, *Polyhedron* **2022**, *213*, 115622.

[39] a) J. S. Danilova, S. M. Avdoshenko, M. P. Karushev, A. M. Timonov, E. Dmitrieva, *J. Mol. Struct.* **2021**, *1241*, 130668; b) N. V. Tverdova, N. I. Giricheva, G. V. Girichev, N. P. Kuz′mina, O. V. Kotova, A. V. Zakharov, *Russ. J. Phys. Chem. A* **2009**, *83*, 2255–2265.

[40] J. F. Brown Jr., *J. Am. Chem. Soc.* **1955**, *77*, 6341–6351.

[41] Y.-P. Jiao, H.-Y. Shi, W.-Y. Zhou, A.-Q. Jia, H.-T. Shi, Q.-F. Zhang, *J. Mol. Struct.* **2022**, *1259*, 132695.

[42] a) S. Celedón, M. Fuentealba, T. Roisnel, I. Ledoux-Rak, J.-R. Hamon, D. Carrillo, C. Manzur, *Eur. J. Inorg. Chem.* **2016**, 3012–3023; b) A. Trujillo, M. Fuentealba, D. Carrillo, C. Manzur, I. Ledoux-Rak, J.-R. Hamon, J.-Y. Saillard, *Inorg. Chem.* **2010**, *49*, 2750–2764.

[43] J. D. Dunitz, L. E. Orgel, A. Rich, *Acta Crystallogr.* **1956**, *9*, 373–375.

[44] J. V. Greenhill, *Chem. Soc. Rev.* **1977**, *6*, 277–294.

[45] P. Gilli, V. Bertolasi, V. Ferretti, G. Gilli, *J. Am. Chem. Soc.* **2000**, *122*, 10405–10417.

[46] R. Taylor, P. A. Wood, *Chem. Rev.* **2019**, *119*, 9427–9477.

[47] V. Artigas, D. Gonzalez, M. Fuentealba, *J. Mol. Struct.* **2017**, *1129*, 325–332.

[48] L. Yang, D. R. Powell, R. P. Houser, *Dalton Trans.* **2007**, 955–964.

[49] a) M. Fuentealba, J.-R. Hamon, D. Carrillo, C. Manzur, *New J. Chem.* **2007**, *31*, 1815–1825; b) A. Trujillo, M. Fuentealba, D. Carrillo, C. Manzur, J.-R. Hamon, *J. Organomet. Chem.* **2009**, *694*, 1435–1440.

[50] a) J. Cisterna, V. Artigas, M. Fuentealba, P. Hamon, C. Manzur, V. Dorcet, J.-R. Hamon, D. Carrillo, *Inorg. Chim. Acta* **2017**, *462*, 266–280; b) J. Cisterna, V. Dorcet, C. Manzur, I. Ledoux-Rak, J.-R. Hamon, D. Carrillo, *Inorg. Chim. Acta* **2015**, *430*, 82–90.

[51] P. Zanello, In *Ferrocenes: Homogeneous Catalysis, Organic Synthesis, Materials Science*, (Eds.: A. Togni, T. Hayashi), VCH: New York, **1995**, Chap. 7, pp. 317–430.

[52] a) I. P. Oliveri, G. Maccarrone, S. Di Bella, *J. Org. Chem.* **2011**, *76*, 8879–8884; b) A. Bugarin, B. T. Connell, *Organometallics* **2008**, *27*, 4357–4369.

[53] a) J. Buey, S. Coco, L. Dıez, P. Espinet †, J. M. Martın-Alvarez, J. A. Miguel, S. Garcıa-Granda, A. Tesouro, I. Ledoux, J. Zyss, *Organometallics* **1998**, *17*, 1750–1755; b) G. Doisneau, G. Balavoine, T. Fillebeen-Khan, J.-C. Clinet, J. Delaire, I. Ledoux, R. Loucif, G. Pucetti, *J. Organomet. Chem.* **1991**, *421*, 299–304.

[54] W. L. F. Armarego, C. L. L. Chai, *Purification of Laboratory Chemicals*, 5th edn.; Butterworth-Heinemann, Elsevier Inc.: Amsterdam, The Netherlands, **2003**.

[55] APEX2, Bruker AXS Inc., Madison, Wisconsin, USA, **2007**.

[56] O. V. Dolomanov, L. J. Bourhis, R. J. Gildea, J. A. K. Howard, H. Puschmann, *J. Appl. Crystallogr.* **2009**, *42*, 339–341.
[57] G. M. Sheldrick, *Acta Crystallogr. Sect. A* **2008**, *64*, 112–122.
[58] H. Le Bozec, T. Le Bouder, O. Maury, A. Bondon, I. Ledoux, S. Deveau, J. Zyss, *Adv. Mater.* **2001**, *13*, 1677–1681.
[59] G. te Velde, F. M. Bickelhaupt, E. J. Baerends, C. Fonseca Guerra, S. J. A. van Gisbergen, J. G. Snijders, T. Ziegler, *J. Comput. Chem.* **2001**, *22*, 931–967.
[60] ADF 2021.1, SCM, Theoretical Chemistry, Vrije Universiteit, Amsterdam, The Netherlands, http://www.scm.com.
[61] E. van Lenthe, E. J. Baerends, J. G. Snijders, *J. Chem. Phys.* **1994**, *101*, 9783–9792.
[62] J. P. Perdew, K. Burke, M. Ernzerhof, *Phys. Rev. Lett.* **1996**, *77*, 3865–3868.
[63] C. Adamo, V. Barone, *J. Chem. Phys.* **1999**, *110*, 6158–6170.
[64] E. Van Lenthe, E. J. Baerends, *J. Comput. Chem.* **2003**, *24*, 1142–1156.
[65] S. Grimme, S. Ehrlich, L. Goerigk, *J. Comput. Chem.* **2011**, *32*, 1456–1465.
[66] A. Klamt, G. Schüürmann, *J. Chem. Soc. Perkin Trans. 2* **1993**, 799–805.
[67] A. Klamt, V. Jonas, *J. Chem. Phys.* **1996**, *105*, 9972–9981.
[68] S. I. Gorelsky, SWizard program, http://www.sg-chem.net/, University of Ottawa, Ottawa, Canada, **2013**.
[69] S. I. Gorelsky, A. B. P. Lever, *J. Organomet. Chem.* **2001**, *635*, 187–196.

Manuscript received: July 26, 2022
Revised manuscript received: September 15, 2022
Accepted manuscript online: October 4, 2022